Electronic Supplementary Information

A mixed ion-electron conducting carbon nanotube ionogel to efficiently harvest heat from both temperature gradient and temperature fluctuation

Hanlin Cheng,[a] Shizhong Yue,[a] Qiujian Le,[a] Qi Qian,[a] Jianyong Ouyang*[a]

[a] *Department of Materials Science and Engineering, National University of Singapore, Singapore 117576, Singapore. E-mail: mseoj@nus.edu.sg*

1. Supplementary figures

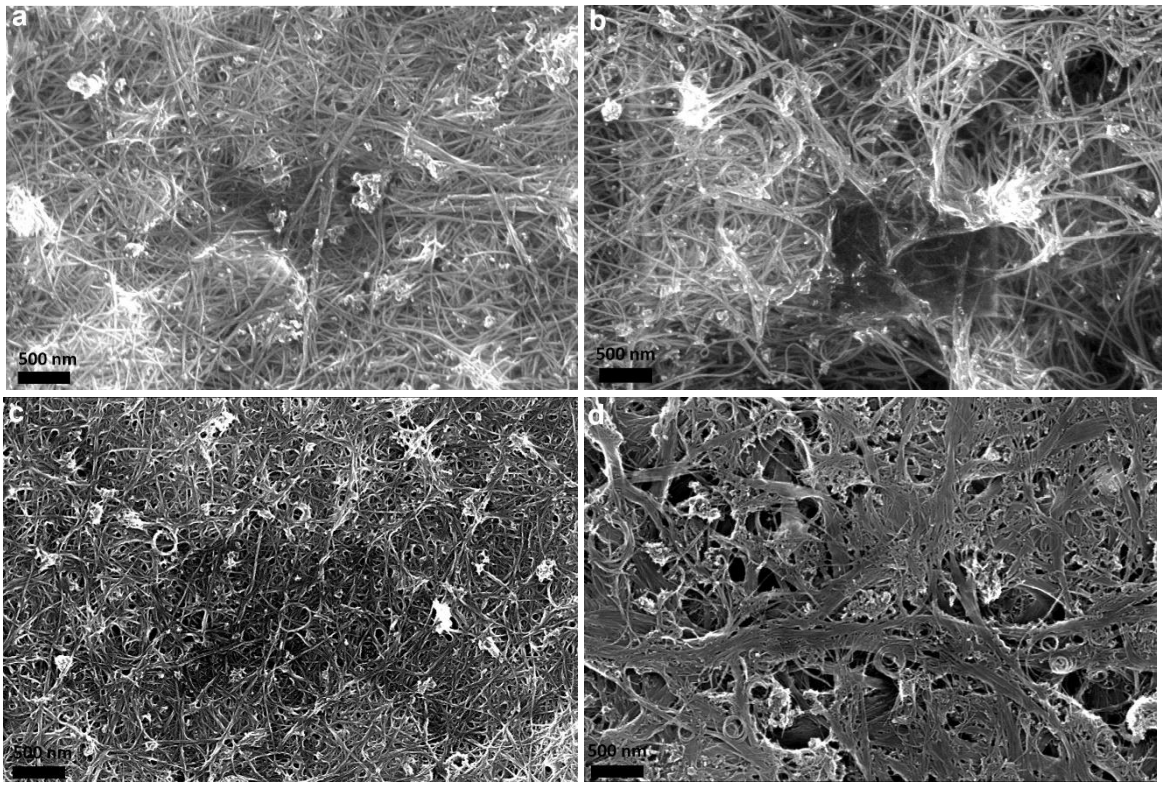

Fig. S1. SEM images of SWNT networks. The SWNT networks were prepared by using hot water to remove SDS, gelatin and ionic liquid from the ionogels with the SWNT loadings of (a) 2 wt.%, (b) 5.4 wt.%, and (c) 8.2 wt.%. (d) SEM image of a SWNT/SDS film prepared from its aqueous dispersion.

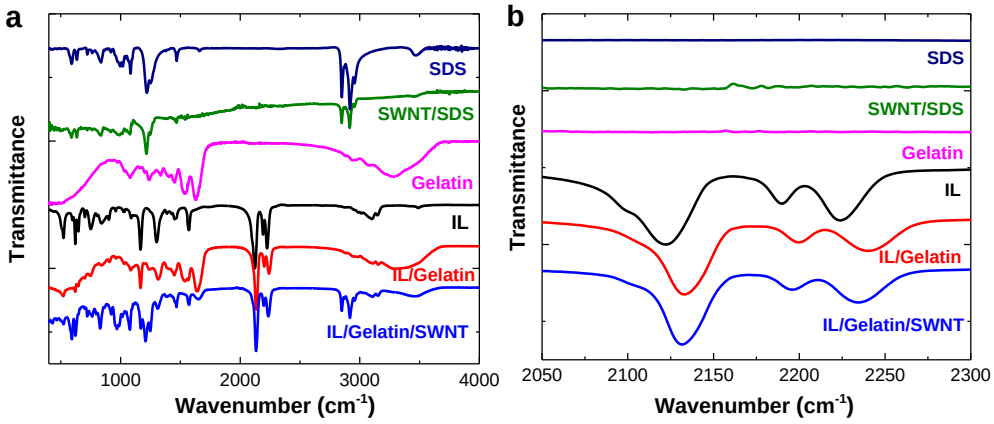

Fig. S2. ATR-FTIR spectra of samples include SWNTs, gelatin, SDS, gelatin ionogel, and SWNT (5.4 wt.%) ionogels in the range of (a) 400 to 4000 cm^{-1}, and (b) 2050 to 2300 cm^{-1}.

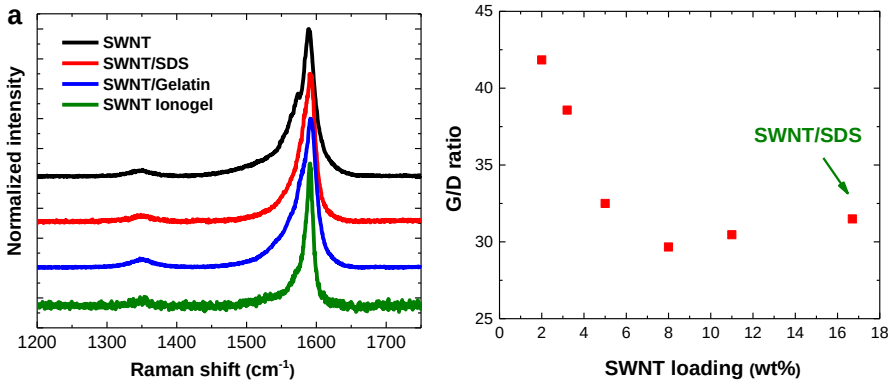

Fig. S3. (a) Raman spectra of SWNTs, SWNT/SDS, SWNT/gelation and SWNT ionogels. (b) Variation of the intensity ratio of the G to D band of the SWNT ionogels with the SWNT loading. The mass loading of SWNTs was 16.7 wt.% in SWNT/SDS.

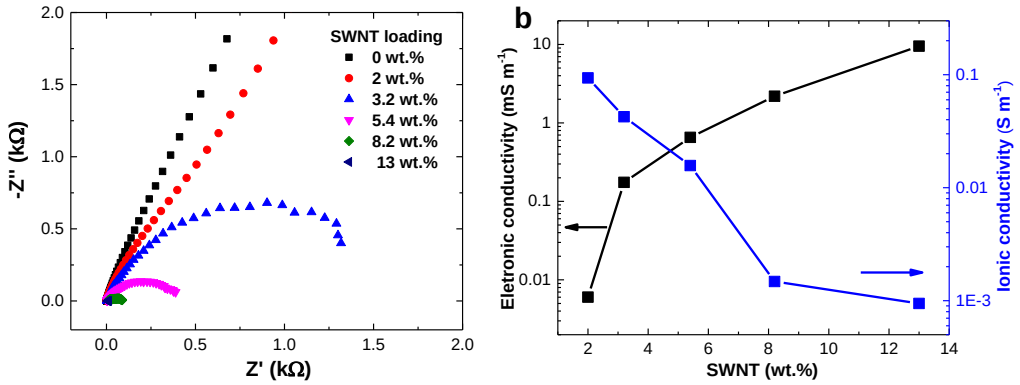

Fig. S4. (a) Nyquist plots of SWNT ionogels with different SWNT loadings. (b) Dependences of the ionic and electronic conductivities of the ionogels on the SWNT loading. The conductivities are presented in log scale.

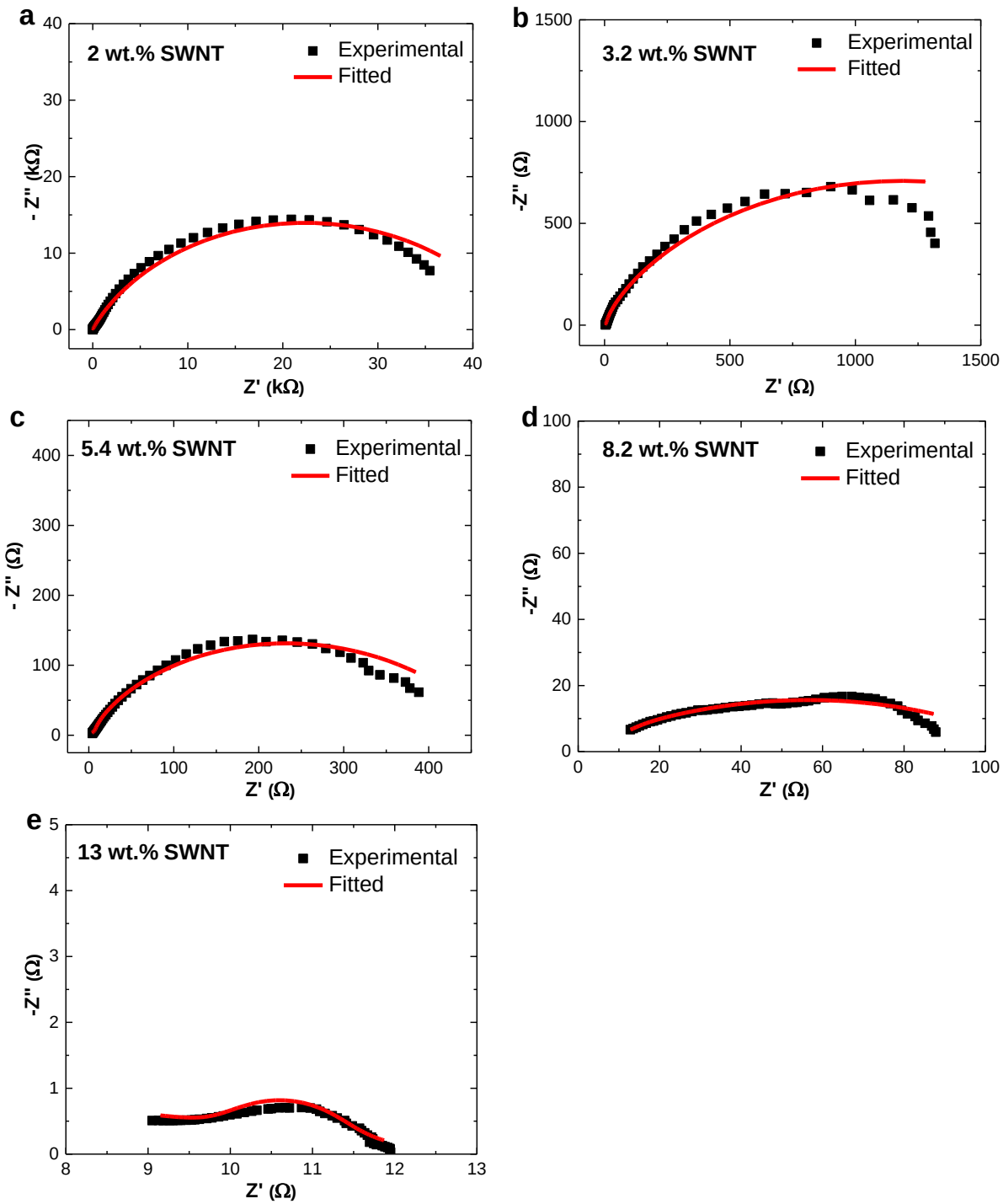

Fig. S5. Fitting of the Nyquist plots of the SWNT ionogels with the SWNTs loadings of (a) 2 wt.%, (b) 3.2 wt.% (c) 5.4 wt.% (d) 8.2 wt.%, and (e) 13 wt.%. The black dots are the experimental results, and red lines are the fittings.

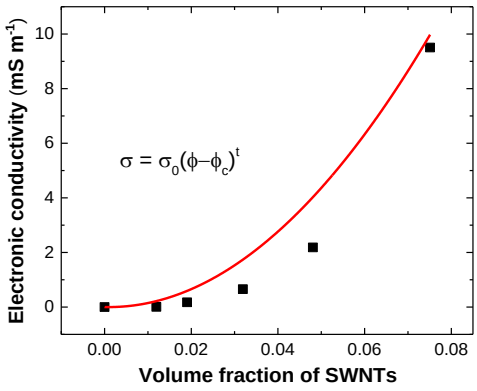

Fig. S6. Fitting of the electronic conductivity of the SWNT ionogels with the percolation model. The black dots are the experimental results, and the red curve is the fitting. The volume fraction was derived from the SWNT loading and the densities of the components of the SWNT ionogels. The densities are 1.9 g cm^{-3} (SWNT), 1.35 g cm^{-3} (gelatin), 1.1 g cm^{-3} (EMIM:DCA), and 1 g cm^{-3} (SDS). The *t* value is assumed as 2 for three-dimensional electron transportation in the SWNT ionogels.

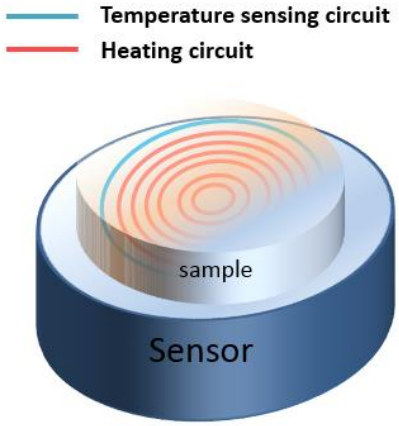

Fig. S7. Schematic illustration of the thermal conductivity measurement. The sample is placed on the top of sensor. The heating circuit locates in the center, and transient temperature change is recorded via the surrounding sensing circuit.

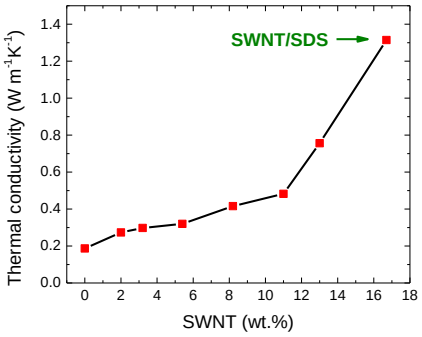

Fig. S8. Variations of the thermal conductivity of the SWNT ionogels with the SWNTs loading. The thermal conductivity of a SWNT/SDS film is presented for comparison. The mass loading of SWNTs was 16.7 wt.% in SWNT/SDS.

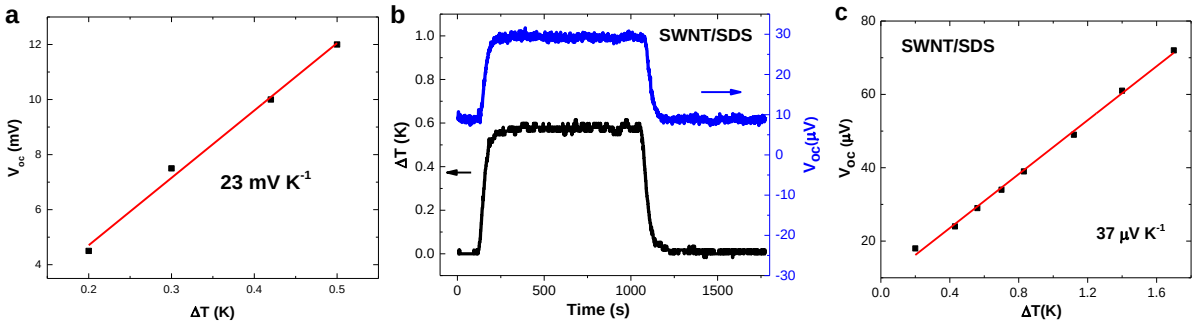

Fig. S9. (a) Thermovoltage of gelatin ionogels without SWNT. (b) Thermovoltage profiles of a SWNT/SDS film prepared from the aqueous dispersion of SWNTs and SDS, and (c) its Seebeck coefficient obtained from the V_{oc}-ΔT relationship.

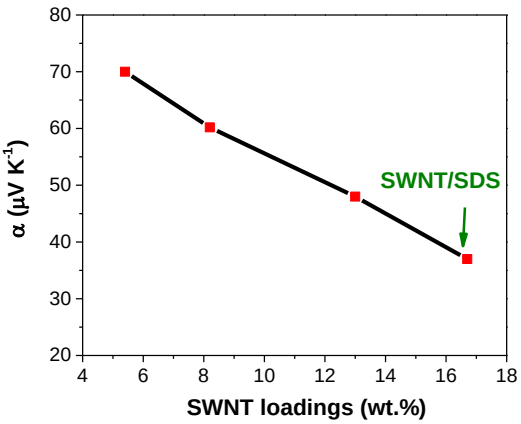

Fig. S10. Variation of the Seebeck coefficient of the SWNT ionogels with the SWNT loading. The Seebeck coefficient values were calculated in terms of the stable open-circuit voltage. The mass loading of SWNTs was 16.7 wt.% in SWNT/SDS.

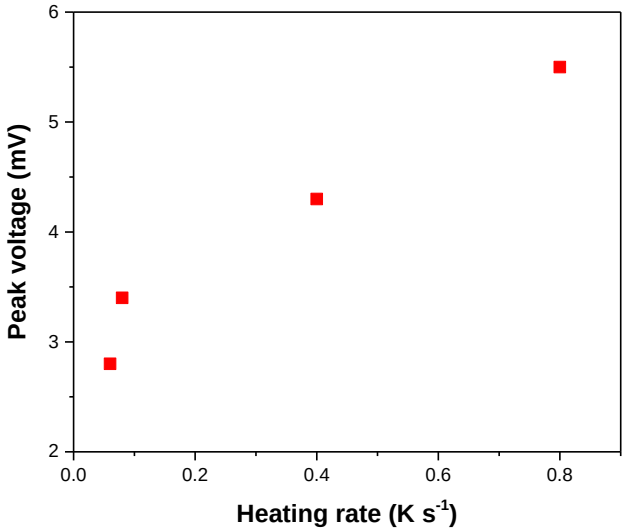

Fig. S11. The dependence of the peak voltage on the heating rate.

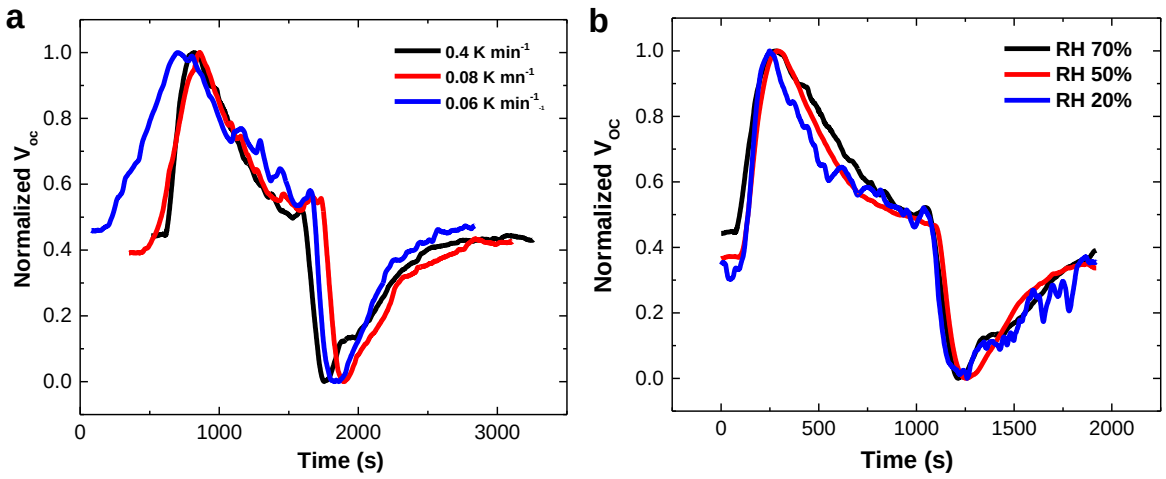

Fig. S12. Normalized thermovoltage profiles of the SWNT ionogels (2 wt.% SWNT). The thermovoltage profiles were obtained under (a) different heating rates, and (b) different humidities. The normalized voltages were obtained by $V = \frac{V - V_{min}}{V_{max} - V_{min}}$, with V, V_{min}, V_{max} is the instant, minimum and maximum thermovoltage, respectively.

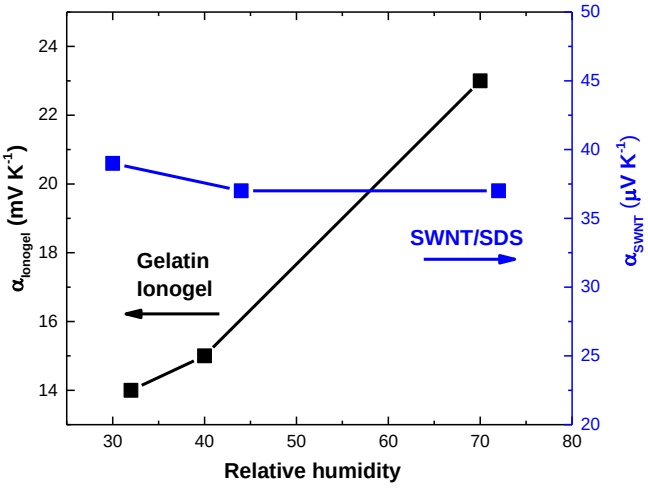

Fig. S13. Humidity effect on the thermovoltage. Dependences of the Seebeck coefficient of SWNT/SDS (blue line) and thermovoltage of gelatin ionogels without SWNT (black line) on the relative humidity.

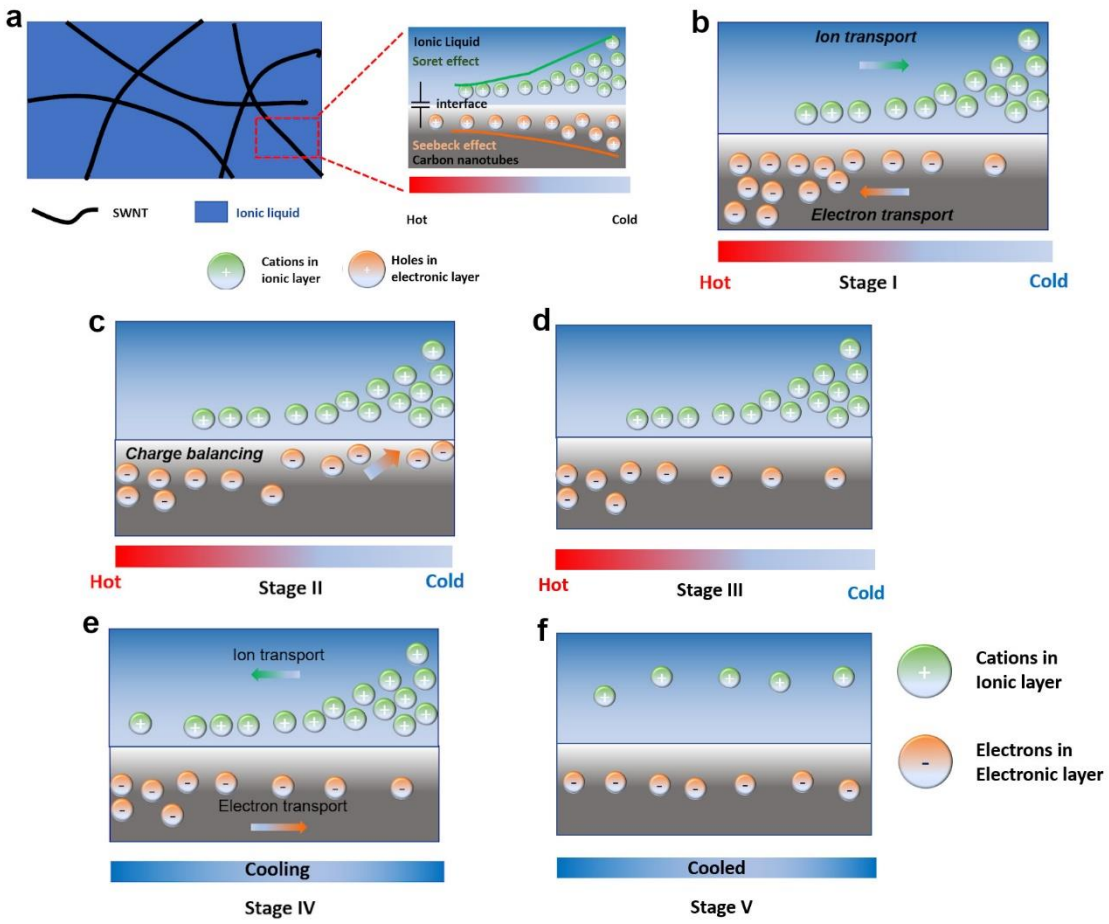

Fig. S14. (a) Schematic illustration of the structure of SWNT ionogels and the interface between electronically conductive SWNTs and ionically conductive IL under temperature gradient. Ion and electron transportations at the (b) stage I, (c) stage II, (d) stage III, (e) stage IV, and (f) stage V.

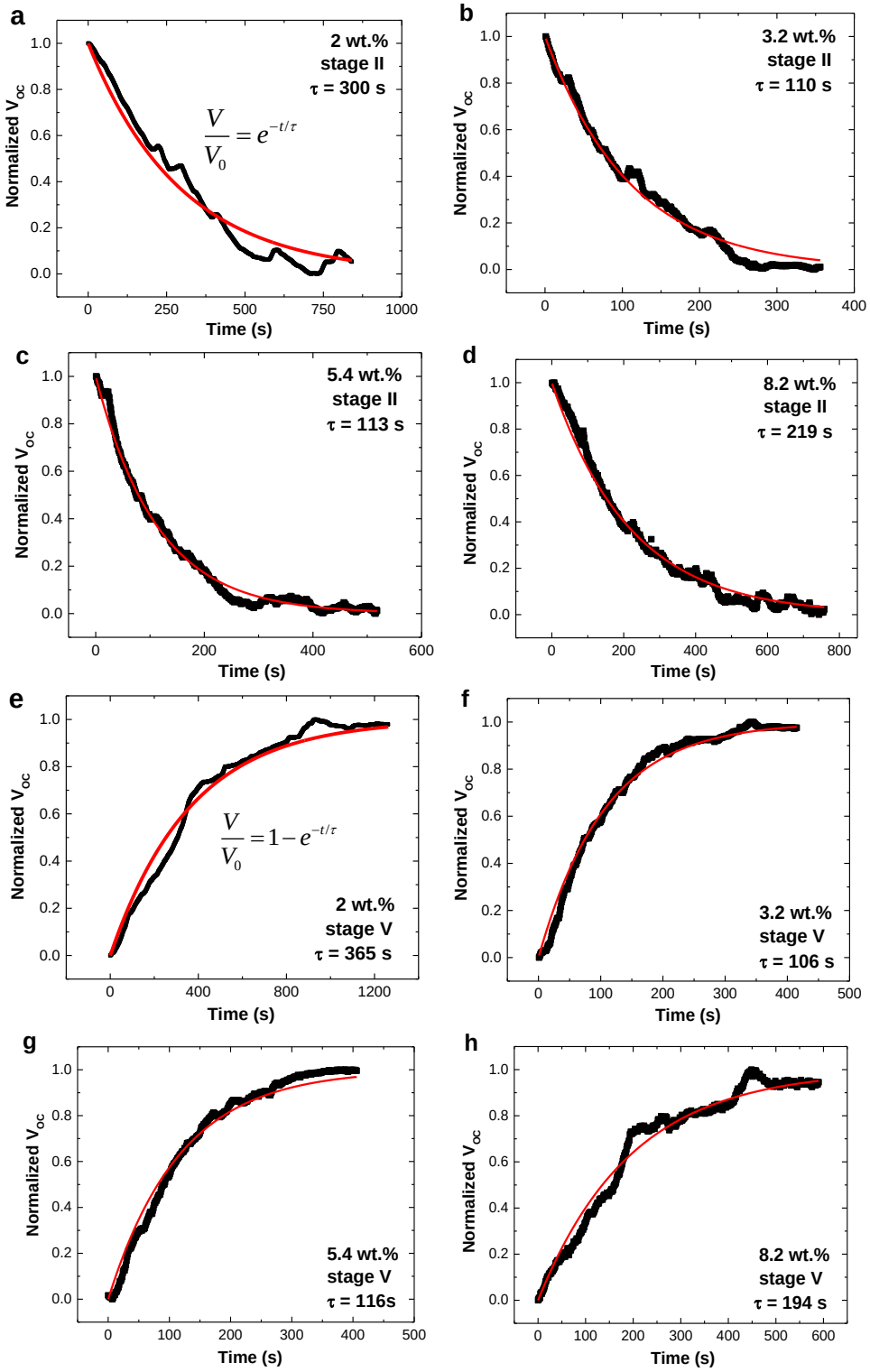

Fig. S15. (a) Schematic illustration of the structure of SWNT ionogels and the interface between electronically conductive SWNTs and ionically conductive IL under temperature gradient. Ion and electron transportations at the (b) stage I, (c) stage II, (d) stage III, (e) stage IV, and (f) stage V.

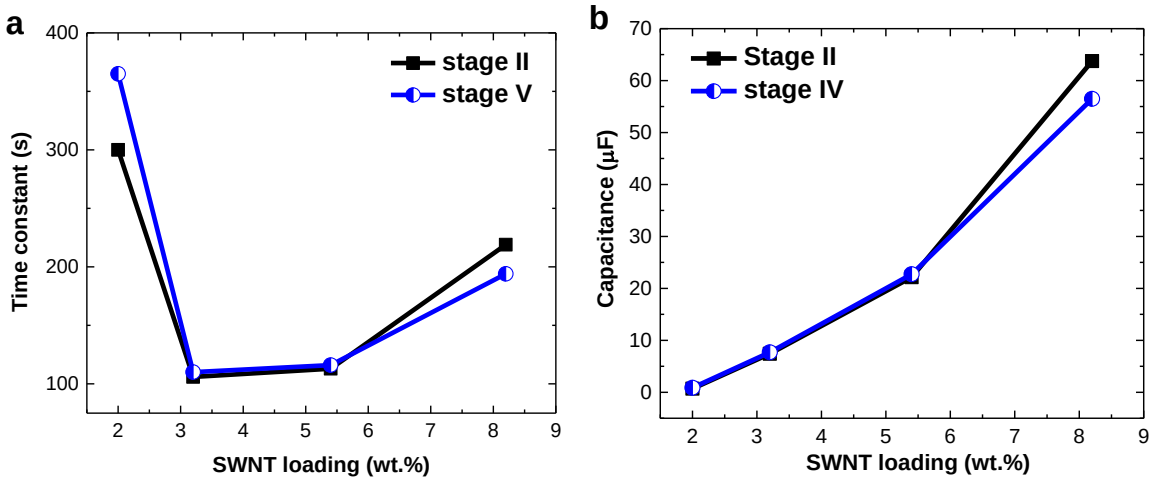

Fig. S16. (a) The time constants, and (b) the capacitances determined by resistance (R_e+ R_{ion}) in the stage II and stage V, respectively.

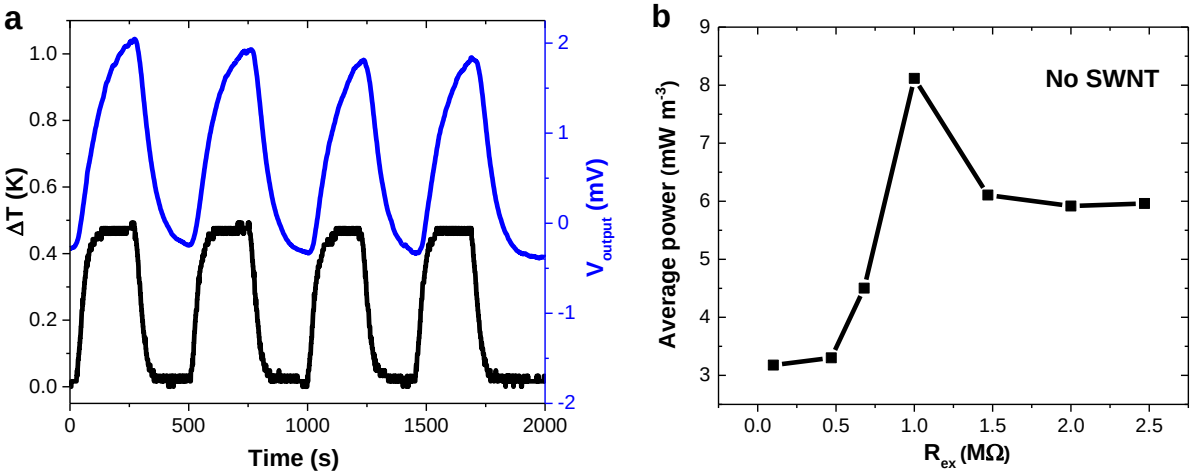

Fig. S17. (a) Output voltage profile on an external load of 680 kΩ connected to an ionic TE capacitor with a gelatin ionogels under rectangular temperature fluctuation. (b) The average power density with different external loads of the gelatin ionogels.

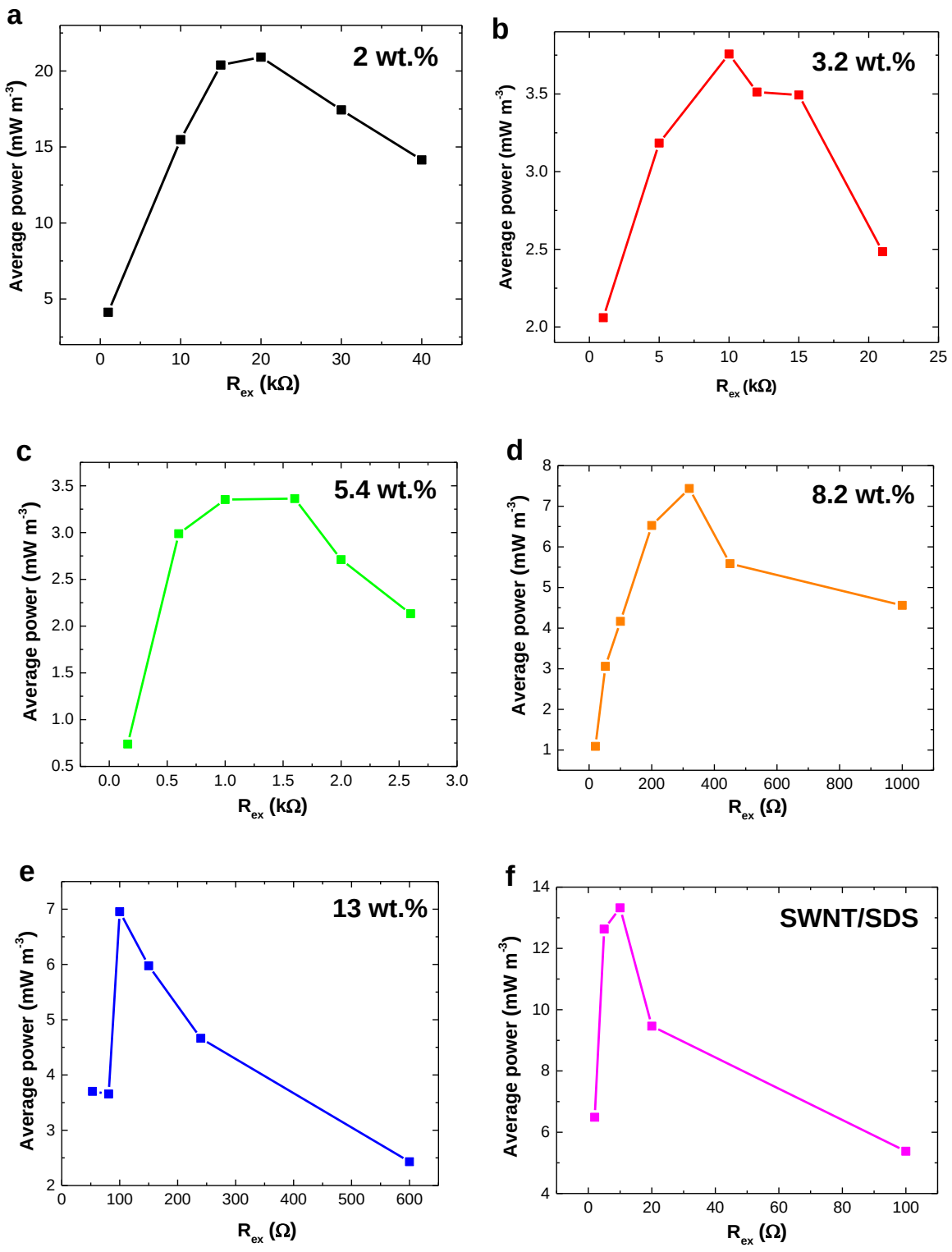

Fig. S18. Variation of the average power density MTECs with the external resistance. SWNT ionogels with different SWNT loadings of (a) 2 wt.%, (b) 3.2 wt.%, (c) 5.4 wt.%, (d) 8.2 wt.%, and (e) 13 wt.% were used. (f) The variation of the average power density of a TE generator with a SWNT/SDS film with the external resistance.

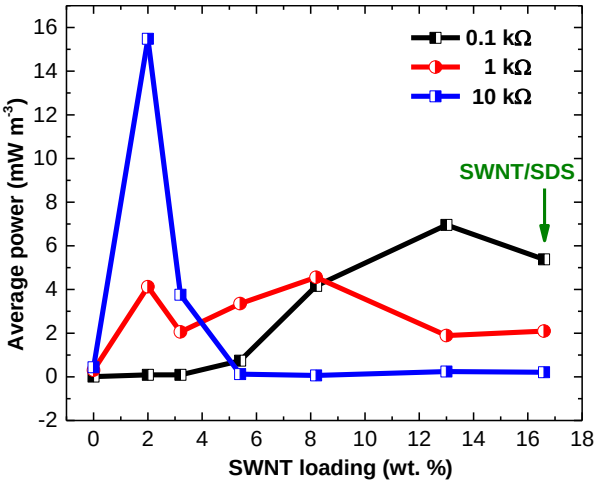

Fig. S19. Variations of the output average power of MTECs with the SWNT loading. An external load with the resistance of 100 Ω, 1 kΩ, or 10 kΩ was connected to MTECs with the ionogels of various SWNT loadings. The average powers of a TE generator with a SWNT/SDS film are presented for comparison.

2. Supplementary notes

Calculation of peak power and average power

The peak (P_{peak}) and average ($P_{average}$) powers of MTECs were calculated in terms of the equations,

$$P_{peak} = \frac{U_{peak}^2}{V\,R_{ex}}, \text{ and} \qquad \text{Equation S1}$$

$$P_{average} = \frac{1}{V\,\Delta t}\int \frac{U^2}{R_{ex}}dt, \qquad \text{Equation S2}$$

where U_{peak} and U are the peak and instantaneous voltages, respectively, on the external load during a thermal cycle, R_{ex} is the resistance of external load, V is the volume of the sample, and Δt is the duration of the thermal cycle.

Heat-to-electricity conversion evaluation

The heat-to-electricity conversion efficiency (η) is in the ratio of energy generated (E_{output}) to the heat input (Q_{in})

$$\eta = \frac{E_{output}}{Q_{in}}, \qquad \text{Equation S3}$$

As stated in paper of *Adv. Electron. Mater.* 2017, 3, 1700013 by Crispin et al.,[1] Q_{in} includes three parts,

$$Q_{in} = \alpha T_H \int_0^{\Delta t} i dt + \lambda A \int_0^{\Delta t} T dt - \frac{1}{2} \int_0^{\Delta t} i^2 R_{in} dt, \qquad \text{Equation S4}$$

Where α is the open circuit thermovoltage. T_H is the temperature at the hot side, i is the current, λ is the thermal conductivity, A the sectional area of the sample, T is the average temperature, R_{in} the internal resistance of the sample, and Δt is the duration of one thermal cycle.

The power density is giver by

$$P_{average} = \frac{\int_0^{\Delta t} i^2 R_{ex} dt}{A \Delta t \Delta l}, \qquad \text{Equation S5}$$

Where Δl is the distance between two electrodes, R_{ex} is the resistance of external load.

The optimal power achieves when R_{ex} closes to R_{in}. We can obtain

$$Q_{in} = 2A\Delta t \Delta l \frac{T_H}{\Delta T} P_{average} + \lambda A \int_0^{\Delta t} T dt - \frac{1}{2} A \Delta t \Delta l P_{average} \qquad \text{Equation S6}$$

Where ΔT is the temperature difference between cold and hot side

By using $E_{output} = A \Delta l \Delta t P_{average}$ in equation (S1), we can obtain

$$\eta = \frac{1}{2\frac{T_H}{\Delta T} + \frac{\lambda \int_0^{\Delta t} T dt}{\Delta l \Delta t P_{average}} - \frac{1}{2}}, \qquad \text{Equation S7}$$

Therefore, higher the $\frac{\Delta l \Delta t P_{average}}{\lambda \int_0^{\Delta t} T dt}$, better the performance of heat-to-electricity conversion. It is thus reasonable to use $\frac{P_{average}}{\lambda}$ to compare the performance of different devices.

Reference

1 H. Wang, D. Zhao, Z. U. Khan, S. Puzinas, M. P. Jonsson, M. Berggren and X. Crispin, *Adv. Electron. Mater.*, 2017, **3**, 1700013.